Self-assembly based on heterotriangulene derivatives: from nanowires to microrods

Xiangjian Wan,[a] Huaqiang Zhang,[b] Yanqin Li[b] and Yongsheng Chen*[a]

Received (in Victoria, Australia) 16th October 2009, Accepted 15th January 2010
First published as an Advance Article on the web 10th February 2010
DOI: 10.1039/b9nj00572b

Compound **SA-6**, **SA-8** and **SA-10** (totally called **SAs**) were synthesized by palladium-catalyzed Sonogashira cross-coupling reactions of core derivative **3** with three equiv. of 1-alkyloxy-4-ethynylbenzene **2** in good yields. After the dichloromethane solutions of **SAs** were mixed with methanol, two-level self-assemblies from nanowires to microrods based on **SAs** were obtained and characterized with scanning electron microscopy (SEM), transmission electron microscopy (TEM) and X-ray diffraction (XRD). The driving force of the two-level self-assembly is attributed to the strong π–π stacking ability of heterotriangulene cores and the hydrophobic interactions of alkyl chains with solvent molecules. These two processes may well be used for other molecules to fabricate new nanomaterials in the field of photoelectric devices.

Introduction

In the past decades, one dimensional (1D) nanomaterials including wires,[1] tubes,[2] rods,[3] and belts[4] have attracted extensive investigations, due to their unique properties and applications in nanoscale devices. However, most researchers have focused on inorganic compounds[1–4] and polymers.[5] Recently, organic nanomaterials based on small molecules have attracted more and more attention, owing to their special properties for use in electronic and optoelectronic nanodevices.[6] Scientists have successfully constructed 1D organic nanostructures with the help of hydrogen-bonding,[7–9] π–π stacking,[10,11] electrostatic interactions,[12,13] and other nonconvalent interactions.[14] Among them, self-assembly of π-conjugated molecules is of extreme importance, and π–π stacking is considered as one of the main driving forces for the formation of 1D assembly.[15] This is particularly evident in the large discotic molecules such as perylene tetracarboxylic diimide (PTCDI) based derivatives,[16,17] which form a unique class of n-type semiconductor in comparison to the more common p-type counterpart in organic semiconductors.[16,17] As a part of our efforts toward synthesizing new organic n-type materials, we have identified heterotriangulene **A** (Chart 1) as a promising candidate in our previous work.[18] The three carbonyl groups of **A** greatly reduce the electron density of the aromatic core, a feature that has been shown to effectively promote π–π interaction,[19] which is important for the conduction of electrons in n-type materials. The electron deficient aromatic core of **A** and its C_3 symmetry also provided us with an excellent platform to investigate the self-assembly of 1D nanostructures. The main challenge of 1D self assembly of molecules based on **A** lies in controlling and optimizing the strong π–π interactions between the aromatic cores in cooperation with the hydrophobic interactions of the alkyl chains linked at the core with solvent molecules.[20] It is reported before that 1D assembly can simply be obtained by dispersing a concentrated solution of a specific compound into a "poor" solvent.[21] And when the molecules have long alkyl side chains, the aggregation often proceeds too fast for the molecular assembly to grow along one direction, thus leading to formation of chunky aggregates rather than nanowires.[22] In this regard, we report the development of a family of n-type semiconductors **SA-6**, **SA-8** and **SA-10** (Chart 1) based on the core **A** at room temperature and their different self-assembly behaviors with different alkyl side chains.

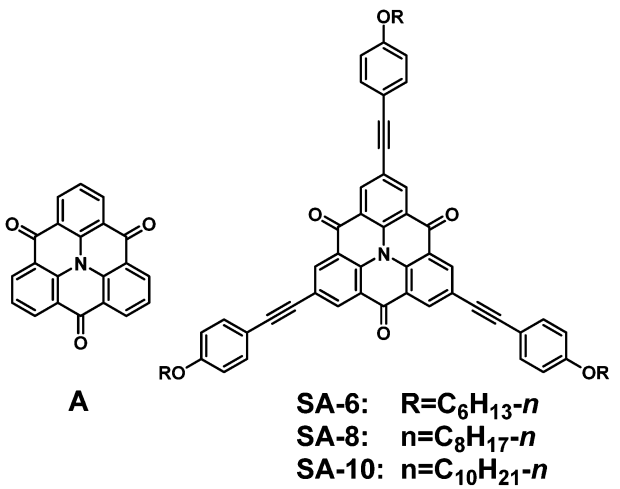

Chart 1 Molecular structures of **A** and **SAs**.

[a] *Key Laboratory for Functional Polymer Materials and Center for Nanoscale Science and Technology, Institute of Polymer Chemistry, College of Chemistry, Nankai University, 300071, Tianjin, China. E-mail: yschen99@nankai.edu.cn; Fax: +86 22 23499992; Tel: +86 22 23500693*
[b] *Lanzhou Petrochemical Research Center, PetroChina, Lanzhou 730060, China*

Results and discussion

Synthesis

Compound **SAs** were synthesized by palladium-catalyzed Sonogashira cross-coupling reaction[23] of core derivative **3**[18] with three equiv. of 1-alkyloxy-4-ethynylbenzene **2**[24] in good yields (Scheme 1). As expected, **SAs** were readily soluble in common organic solvents such as toluene, CH_2Cl_2, and THF.

Thermal analysis

Thermal stabilities of **SAs** were investigated with thermogravimetric analysis (TGA), as shown in Fig. 1. The onset decomposition temperatures of the molecules decrease from **SA-6** to **SA-10**, indicating that the longer alkyl side chains lead to the weaker intermolecular interactions from **SA-6** to **SA-10** in the solid state. Even this, the onset decomposition temperatures of the molecules are all around 400 °C in nitrogen, illustrating that they are quite thermally stable and can be used for various high-temperature processes in the construction of electronic devices.

The different extent of π–π stacking for **SAs** was also evidenced by the measurement of Differential scanning calorimetry (DSC), as shown in Fig. 2. The DSC patterns of **SAs** show only one phase transition on heating at 187, 180, 166 °C from **SA-6** to **SA-10**, respectively, which corresponds to their melt points. The dramatically lower melting point from **SA-6** to **SA-10** indicates the weakened molecular stacking, which is caused by the longer alky side chains from **SA-6** to **SA-10**.

Optical properties

The absorption spectra from **SA-6** to **SA-10** (Fig. 3) in dichloromethane show intensive transitions in the UV region, with strong absorption bands in the range of 230–310 nm. These bands are assigned to the π–π* transitions of subunits **2**. The absorption spectra of **SAs** show a maximum at 348 nm with a well-resolved vibronic structure, which can be assigned to the transition of core part according to the reported literature.[25] Apart from the characteristic absorptions of the **A** core and the subunits **2**, the solution spectra of these three compounds also show a new broad band at longer wavelength around 458 nm, which depends on their effective conjugation lengths.[26] To gain further insight into the interactions between the molecules in solid state, we investigated the absorption behaviors of **SAs** in films. The film absorption results from **SA-6** to **SA-10** are nearly the same, so herein, we take **SA-6** as an example to compare with its absorptions in solution. As shown in Fig. 3, the spectrum of **SA-6** exhibits a bathochromic-shift in the solid state compared with that in solution, *i.e.*, from wavelength of 458 nm in solution shifted to 472 nm in film. Since the probability of assembling for aggregates of **SA-6** in the solid matrix increases, one may perceive that the bathochromic-shift phenomenon is coming from the intermolecular π–π interactions of **SA-6** in solid state. The bathochromic shift of UV absorption from solution to film also suggests that the aggregation style of **SA-6** in solid state is not exact π–π stacking.[27]

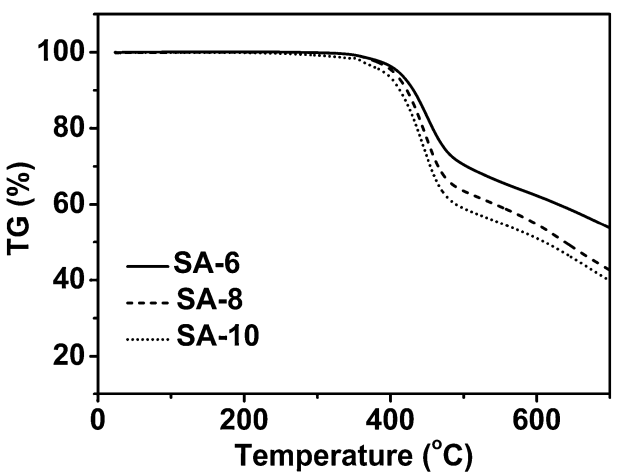

Fig. 1 TGA plots of **SAs** with a heating rate of 10 °C min^{-1} under N_2 atmosphere.

The fluorescence spectra of **SAs** at the same concentration, show structured emission bands around 382 nm and broad featureless emission bands at 500 nm, when all excited at 348 nm (Fig. 4), which is in accordance with the result in literature.[19] The emission bands around 382 nm, showing normal Stoke shift of 34 nm and the same emission intensity, can be assigned to the locally excited state emissions of **SAs**.[28] But it is very interesting to find that the band intensities at 500 nm decrease with the increasing length of the alkyl chains.

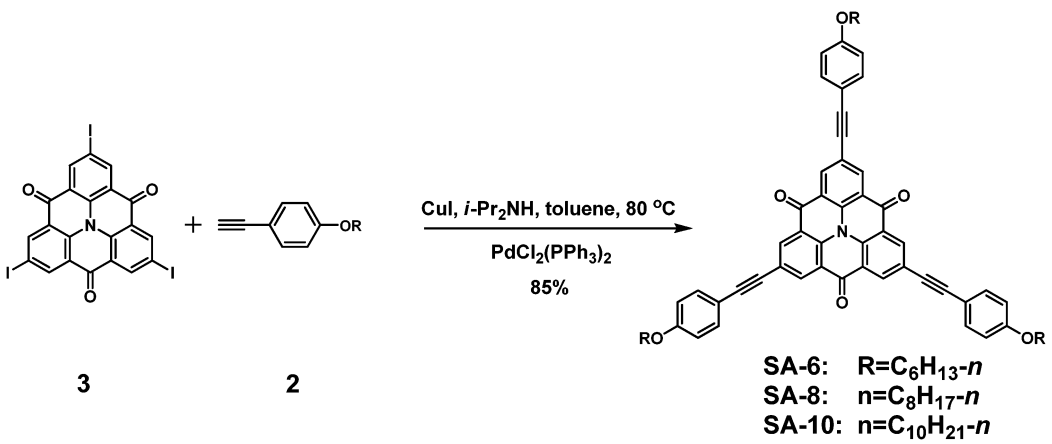

Scheme 1 The synthesis of **SAs**.

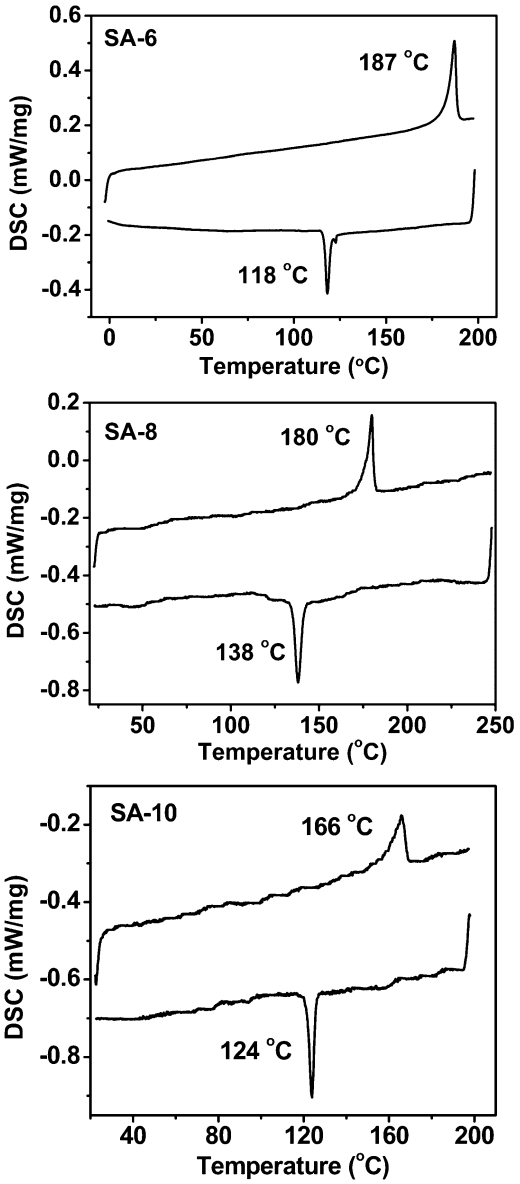

Fig. 2 Differential scanning calorimetry (DSC) traces of **SAs** with a heating/cooling rate of 5 °C min^{-1}. The data shown are from the second heating-cooling cycle.

To deeply explore the origin of the band at 500 nm, we also measured the fluorescence of **SA-6** (take for example in Fig. 5) in dichloromethane with different concentrations. It was found that the emission intensity ratio for band around 382 nm *versus* band at 500 nm showed apparent concentration dependence. With the increase of concentration of **SA-6**, the band intensities at 500 nm increase while those around 382 nm show common features of concentration quenching. These results also illustrated that the band at 500 nm may originate from the intermolecular aggregation and can be assigned to the excimer emissions.

Electronchemical properties

In view of the potential application of such molecules in optoelectronics, it is important to consider the relative highest occupied and lowest unoccupied molecular orbital (HOMO and LUMO) parameters, which indicate the facility to inject

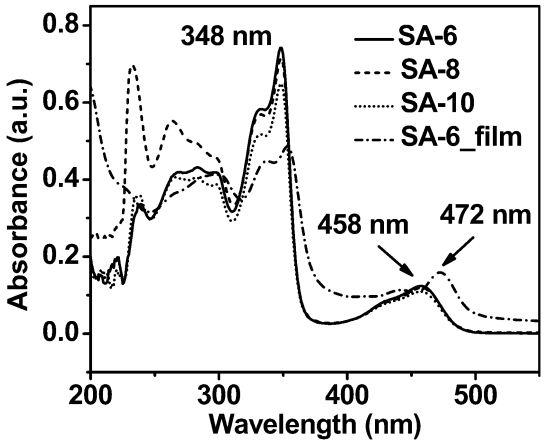

Fig. 3 The absorption spectra of **SAs** (1.0×10^{-6} M) in dichloromethane and **SA-6** in thin film.

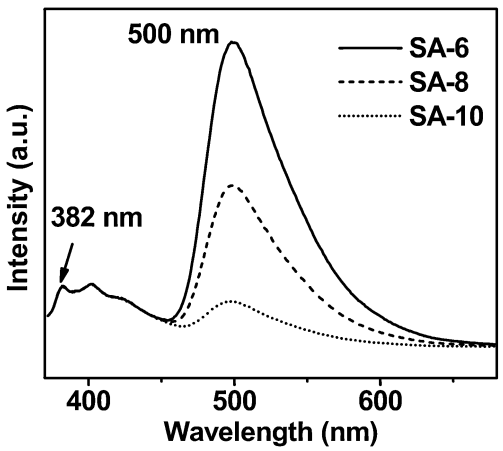

Fig. 4 Uncorrected emission spectra of **SAs** (λ_{ex} = 348 nm) in dichloromethane (5.0×10^{-7} M).

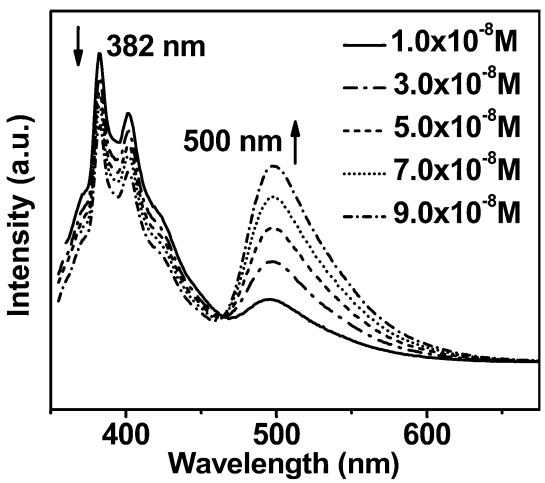

Fig. 5 Uncorrected emission spectra of **SA-6** (λ_{ex} = 348 nm) in dichloromethane with different concentrations.

holes and electrons respectively in the material. Cyclic voltammetry (CV) was carried out to obtain the electronic levels of **SAs** (Fig. 6). All these compounds have two irreversible reduction peaks. So we take **SA-6** for example to calculate its HOMO and LUMO. A LUMO level of −3.44 eV for **SA-6** was calculated from the onset value of the reduction peak ($E^{\text{onset}}_{\text{red}}$ = −1.36 V *versus* Fc/Fc^{+}). With the optical band-gap of 2.5 eV (from onset wavelength of the UV-vis spectrum of **SA-6** in solid state), the HOMO level of −5.94 eV for **SA-6** has been calculated.[29]

Self assembly properties

The self-assemblies of **SAs** were performed using a diffusion process in a binary solvent of dichloromethane–methanol,

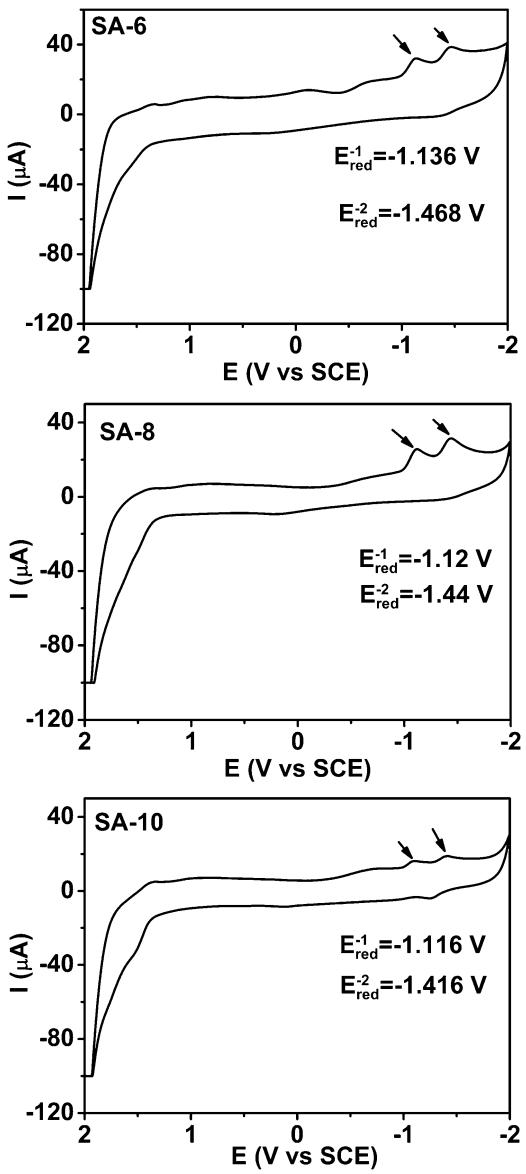

Fig. 6 Cyclic voltammograms of **SAs** in 0.1 M Bu_4NPF_6–CH_2Cl_2, with a glassy carbon electrode at a scan rate of 100 mV s^{-1}. A platinum wire and an SCE was used as the counter and reference electrode, respectively.

which enables effective molecular aggregation into well-organized nanowires and microrods, as evidenced by the optical spectral measurements below. In SEM images (Fig. 7), self-assemblies of **SAs** as many microrods, with average diameters of 10 μm and lengths of several millimetres were observed. TEM imaging gave a deeper insight about the structure of the microrods. From the TEM images (Fig. 8), we could find that the microrods are made of straight nanowires packed side by side. The typical width of these nanowires is *ca.* 3 nm. Thus, a two-level self-assembly process may exist in the formation of the microrods based on **SAs**. The first level is due to the strong intermolecular π–π interactions between the large **A** cores, where the molecules assemble along the axis direction of the nanowires. Then, these nanowires assemble in the orthogonal direction of the axis to form the microrods. The driving force for the second level assembly is believed to come from the hydrophobic interactions of alkyl chains with solvent molecules.[30]

Identification and unequivocal assignment of the self-assembly of **SAs** were finally achieved by X-ray diffraction (XRD) and small angle X-ray scattering (SAXS) (Fig. 9). In the wide-angle region, features have been observed corresponding to various short-range interactions. First, at d = 3.4 Å, a relatively sharp scattering was observed, corresponding to the π stacking distance of the large flat **A** cores along the 1D assembly columnar axis (schematic illustration shown in Fig. 10). This is also supported by the single crystal X-ray data of the parent compound heterotriangulene **A**, where the molecules pack into a 1D column with a stacking distance of 3.5 Å.[19,31] The broadening peak at 3.4 Å suggests that either the stacking is less regular or that the **A** cores are slightly tilted with respect to the columnar axis.[32] Then, a large broad and diffuse scattering centered 3.7–4.3 Å was visible, which reflects the short-range correlations of the alkyl chains from **SA-6** to **SA-10**. In the slightly lower angle region, another weak diffuse scattering peak corresponding to a distance of *ca.* 9.0 Å was attributed to some correlations of alkyl chains between neighboring molecules. In the small-angle region, a sharp reflection peak at 2θ = 3.41° was detected (take **SA-6** for example), from which a spacing of a = 25.9 Å was estimated. This value corresponds to the spacing between the lateral 2D arrays. The sharpness and intensity of the small-angle reflection at 2θ = 3.41° indicate clearly the long-range second level assembly between the 1D assembly columns, which is formed by the first-level assembly of **SA-6** due to the intermolecular π–π interactions of **A** cores. Overall, the two-level self-assembly process can be illustrated in Fig. 10.

Conclusion

Due to the π–π stacking interactions of **A** cores and the hydrophobic interactions of alkyl chains with solvent molecules, compound **SAs** could self-assemble into supramolecular organizations from straight nanowires to well-organized microrods through a two-level self-assembly process. This process may well be used for other molecules to fabricate new nanomaterials in the field of photoelectric devices.

Fig. 7 SEM images of self-assemblies of **SA-6** (a), **SA-8** (b) and **SA-10** (c).

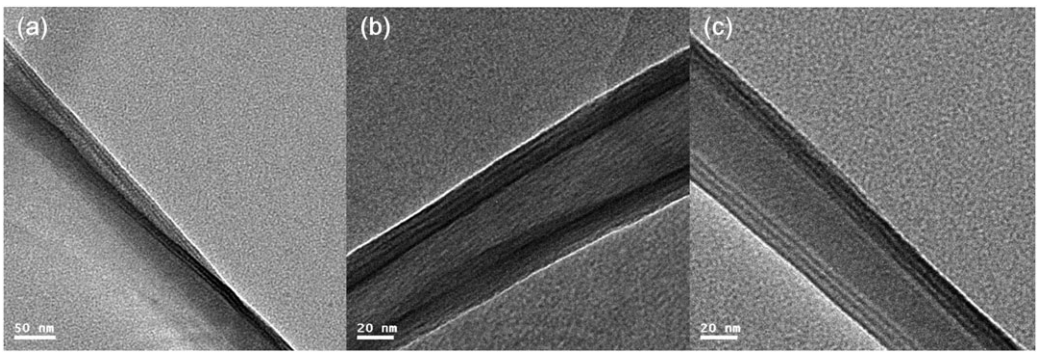

Fig. 8 TEM images of self-assemblies of **SA-6** (a), **SA-8** (b) and **SA-10** (c).

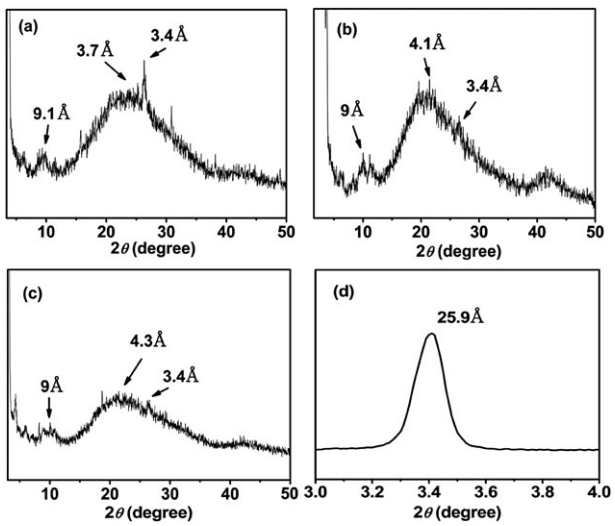

Fig. 9 XRD patterns of self-assemblies of **SA-6** (a), **SA-8** (b), **SA-10** (c) and the SAXS pattern of self-assembly of **SA-6** (d) at room temperature.

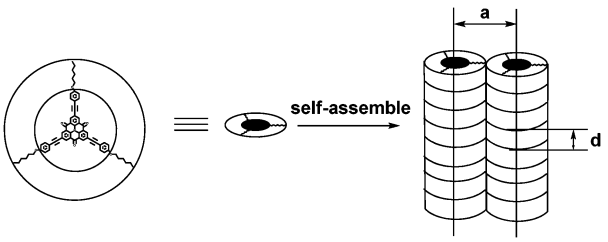

Fig. 10 Schematic illustration of possible molecular arrangements for self-assembly of **SA-6**.

Experimental

General information

Unless stated otherwise, all chemicals and reagents were purchased reagent grade and used without further purification. Solvents were purified by standard methods. All manipulations were performed under a dry Argon atmosphere using standard Schlenk techniques.

^{1}H NMR and ^{13}C NMR spectra were recorded on a Bruker AC-300 Spectrometer. Chemical shifts δ, were reported in parts per million relative to the internal standard TMS. High resolution mass spectra (HRMS) were recorded on a VG ZAB-HS mass spectrometer. UV/Vis spectra were measured on a JASCO V-570 spectrophotometer in a 1 cm width cell. Fluorescence spectra were measured on a JOBIN YVON HORIBA fluorescence spectrophotometer in a 1 cm width cell. Cyclic voltammetry (CV) measurement was performed on an LK98B II Microcomputer-based Electrochemical Analyzer at room temperature with a three-electrode cell in a solution of Bu_4NPF_6 (0.1 M) in dichloromethane at a scanning rate of 100 mV s^{-1}. A platinum wire was used as a counter electrode, and an SCE electrode was used as a reference electrode. After measurement, the reference electrode was calibrated with ferrocene (Fc). Thermogravimetric analysis (TGA) measurement was performed on a TA instrument SDT-TG Q600 under an atmosphere of N_2 at a heating rate of 10 °C min^{-1}. Scanning electron microscopy (SEM) analysis was carried on a Hitachi S-3500N scanning electron microscope at an accelerating voltage of 20 kV. Transmission electron microscopy (TEM) images were performed using a Tecnai 20 at an

accelerating voltage of 200 kV. A 200 kV JEOL 2010F was used for elemental mapping. X-ray diffraction (XRD) experiment was performed on a Rigaku D/max-2500 X-ray powder diffractometer with Cu-Kα radiation (λ = 1.5406 Å) at a generator voltage of 40 kV and a current of 100 mA. SAXS experiments were performed on a Bruker NanoStar SAXS system (Cu-Kα radiation source at a voltage of 40 kV and a current of 35 mA).

Synthesis of compounds

Triketone (**3**)[18] and 1-(akyloxy)-4-ethynylbenzene (**2**)[24] were prepared according to previously reported procedures and showed identical spectroscopic properties to those reported therein.

Compound SA-6. 3 (700 mg, 1 mmol), **2** (810 mg, 4 mmol), CuI (38 mg, 0.2 mmol), $PdCl_2(PPh_3)_2$ (70 mg, 0.1 mmol) were.added to a mixture of *i*-Pr_2NH and toluene (v/v = 1 : 3) (30 mL). The mixture was stirred at 80 °C for 24 h. After cooling to room temperature, the black mixture was filtered through a thin pad of silica gel and the solid on silica gel was washed thoroughly with CH_2Cl_2. The filtrate was evaporated under vacuum. The residue was purified by flash chromatography on silica (CH_2Cl_2/Hexane = 1 : 2) to obtain the pure compound as orange brown solid (0.99 g, 70%). ^{1}HNMR ($CDCl_3$, TMS, 300 MHz, ppm) δ = 8.97(6 H, s, ArH), 7.48 (6.H, d, J = 8.7 Hz, ArH), 6.87 (6 H, d, J = 8.7 Hz, ArH), 3.98 (6 H, t, J = 6.5 Hz, OCH_2), 1.86–1.77 (6 H, m, CH_2), 1.50–1.34 (18 H, m, $(CH_2)_3$), 0.93 (9 H, t, J = 6.8 Hz, CH_3). ^{13}C NMR($CDCl_3$, 75 MHz, ppm): 174.58, 159.80, 136.38, 135.61, 133.39, 123.08, 122.16, 114.55, 113.91, 93.35, 85.29, 68.12, 31.62, 29.19, 25.71, 22.60, 14.01. HRMS (MALDI) m/z 924.4279 ($C_{63}H_{58}NO_6$ $[M+H]^+$ requires 924.4264).

Compound SA-8. ^{1}HNMR ($CDCl_3$, TMS, 300 MHz, ppm) δ = 8.94 (6 H, s, ArH), 7.47 (6 H, d, J = 8.7 Hz, ArH), 6.85 (6.H, d, J = 8.8 Hz, ArH), 3.96 (6 H, t, J = 6.6 Hz, OCH_2), 1.86–1.76 (6 H, m, CH_2), 1.49–1.25 (30 H, m, $(CH_2)_5$), 0.91 (9.H, t, J = 6.9 Hz, CH_3). ^{13}C NMR($CDCl_3$, 75 MHz, ppm): 173.89, 159.54, 135.85, 134.94, 133.24, 122.62, 121.82, 114.27, 113.802, 93.19, 85.21, 68.01, 31.87, 29.67, 29.48, 29.28, 26.05, 22.67, 14.085. HRMS (MALDI) m/z 1008.5214 ($C_{69}H_{70}NO_6$ $[M + H]^+$ requires 1008.5203).

Compound SA-10. ^{1}HNMR ($CDCl_3$, TMS, 300 MHz, ppm) δ = 8.97 (6 H, s, ArH), 7.49 (6 H, d, J = 8.7 Hz, ArH), 6.87 (6.H, d, J = 8.8 Hz, ArH), 3.97 (6 H, t, J = 6.5 Hz, OCH_2), 1.86–1.76 (6 H, m, CH_2), 1.49–1.22 (42 H, m, $(CH_2)_7$), 0.90 (9.H, t, J = 6.9 Hz, CH_3). ^{13}C NMR ($CDCl_3$, 75 MHz, ppm): 174.24, 159.68, 136.14, 135.28, 133.32, 122.86, 122.01, 114.43, 113.86, 93.31, 85.26, 68.08, 31.92, 29.62, 29.56, 29.49, 29.35, 29.26, 26.06, 22.68, 14.09. HRMS (MALDI) m/z 1092.6156 ($C_{75}H_{82}NO_6$ $[M + H]^+$ requires 1092.6142).

Acknowledgements

We gratefully acknowledge the financial support from the National Natural Science Foundation of China. (#50933003, #50902073, #50903044,#20774047), Ministry of Science and Technology (#2006CB932702) and Natural Science Foundation of Tianjin City (#07JCYBJC03000, #08JCZDJC25300).

Notes and references

1 X. F. Duan, Y. Huang, Y. Cui, J. F. Wang and C. M. Lieber, *Nature*, 2001, **409**, 66–69.
2 S. Iijima, *Nature*, 1991, **354**, 56–58.
3 W. U. Huynh, J. J. Dittmer and A. P. Alivisatos, *Science*, 2002, **295**, 2425–2427.
4 Z. W. Pan, Z. R. Dai and Z. L. Wang, *Science*, 2001, **291**, 1947–1949.
5 C. R. Martin, *Acc. Chem. Res.*, 1995, **28**, 61–68.
6 Y. S. Zhao, H. B. Fu, A. D. Peng, Y. Ma, D. B. Xiao and J. N. Yao, *Adv. Mater.*, 2008, **20**, 2859–2876.
7 T. Naddo, Y. K. Che, W. Zhang, K. Balakrishnan, X. M. Yang, M. Yen, J. C. Zhao, J. S. Moore and L. Zang, *J. Am. Chem. Soc.*, 2007, **129**, 6978–6979.
8 T. E. Kaiser, H. Wang, V. Stepanenko and F. Wurthner, *Angew. Chem., Int. Ed.*, 2007, **46**, 5541–5544.
9 A. Ajayaghosh, S. J. George and A. Schenning, *Top. Curr. Chem.*, 2005, **258**, 83–118.
10 H. B. Liu, Y. L. Li, L. Jiang, H. Y. Luo, S. Q. Xiao, H. J. Fang, H. M. Li, D. B. Zhu, D. P. Yu, J. Xu and B. Xiang, *J. Am. Chem. Soc.*, 2002, **124**, 13370–13371.
11 H. B. Liu, Y. L. Li, S. Q. Xiao, H. Y. Gan, T. G. Jiu, H. M. Li, L. Jiang, D. B. Zhu, D. P. Yu, B. Xiang and Y. F. Chen, *J. Am. Chem. Soc.*, 2003, **125**, 10794–10795.
12 D. Q. Wu, L. J. Zhi, G. J. Bodwell, G. L. Cui, N. Tsao and K. Mullen, *Angew. Chem., Int. Ed.*, 2007, **46**, 5417–5420.
13 E. Bellacchio, R. Lauceri, S. Gurrieri, L. M. Scolaro, A. Romeo and R. Purrello, *J. Am. Chem. Soc.*, 1998, **120**, 12353–12354.
14 H. B. Liu, Q. Zhao, Y. L. Li, Y. Liu, F. S. Lu, J. P. Zhuang, S. Wang, L. Jiang, D. B. Zhu, D. P. Yu and L. F. Chi, *J. Am. Chem. Soc.*, 2005, **127**, 1120–1121.
15 J. P. Hill, W. S. Jin, A. Kosaka, T. Fukushima, H. Ichihara, T. Shimomura, K. Ito, T. Hashizume, N. Ishii and T. Aida, *Science*, 2004, **304**, 1481–1483.
16 C. R. Newman, C. D. Frisbie, D. A. da Silva, J. L. Bredas, P. C. Ewbank and K. R. Mann, *Chem. Mater.*, 2004, **16**, 4436–4451.
17 B. Q. Xu, X. Y. Xiao, X. M. Yang, L. Zang and N. J. Tao, *J. Am. Chem. Soc.*, 2005, **127**, 2386–2387.
18 H. Q. Zhang, S. M. Wang, Y. Q. Li, B. Zhang, C. X. Du, X. J. Wan and Y. S. Chen, *Tetrahedron*, 2009, **65**, 4455–4463.
19 J. E. Field and D. Venkataraman, *Chem. Mater.*, 2002, **14**, 962–964.
20 H. Q. Zhang, Y. Q. Li, X. J. Wan and Y. S. Chen, *Chem. Phys. Lett.*, 2009, **479**, 117–119.
21 K. Balakrishnan, A. Datar, R. Oitker, H. Chen, J. M. Zuo and L. Zang, *J. Am. Chem. Soc.*, 2005, **127**, 10496–10497.
22 K. Balakrishnan, A. Datar, T. Naddo, J. L. Huang, R. Oitker, M. Yen, J. C. Zhao and L. Zang, *J. Am. Chem. Soc.*, 2006, **128**, 7390–7398.
23 K. Sonogashira, Y. Tohda and N. Hagihara, *Tetrahedron Lett.*, 1975, **16**, 4467–4470.
24 Y. N. Li, Y. L. Wu, P. Liu, Z. Prostran, S. Gardner and B. S. Ong, *Chem. Mater.*, 2007, **19**, 418–423.
25 D. Hellwinkel and D. Melan, *Chem. Ber.*, 1971, **104**, 1001–1016.
26 J. Rissler, *Chem. Phys. Lett.*, 2004, **395**, 92–96.
27 W. I. Gruszecki, *J. Biol. Phys.*, 1991, **18**, 99–109.
28 N. Rajendiran, K. Sivakumar and T. Stalin, *Spectrochim. Acta, Part A*, 2005, **62**, 991–999.
29 J. Pommerehne, H. Vestweber, W. Guss, R. F. Mahrt, H. Bässler, M. Porsch and J. Daub, *Adv. Mater.*, 1995, **7**, 551–554.
30 M. In, O. Aguerre-Chariol and R. Zana, *J. Phys. Chem. B*, 1999, **103**, 7747–7750.
31 S. Kumar, *Chem. Soc. Rev.*, 2006, **35**, 83–109.
32 B. Alameddine, O. F. Aebischer, W. Amrein, B. Donnio, R. Deschenaux, D. Guillon, C. Savary, D. Scanu, O. Scheidegger and T. A. Jenny, *Chem. Mater.*, 2005, **17**, 4798–4807.

